Long Wavelength Astrophysics

by

Liam Dean Connor

A thesis submitted in conformity with the requirements
for the degree of Doctor of Philosophy
Graduate Department of Astronomy and Astrophysics
University of Toronto

—

Contents

List of Tables

Chapter 1

Pulse Microstructure

1.1 Chapter Overview

In this chapter we present results from full-polarization single-pulse studies of pulsar B0329+54 observed with the Algonquin Radio Observatory 46 m telescope. We find microstructure to be a generic property of individual pulses between 400-800 MHz. We also analyze B0329+54's quasi-periodic structure using a reduced autocorrelation function (rACF). Unlike in other pulsars, we do not find a characteristic timescale in its quasi-periodicity, although the range of of periods is consistent with the known $t_\mu \approx 6 \times 10^{-4} P$ and $T_\mu \approx 10^{-3} P$ relations. Our polarimetry results agree with Mitra et al. (2015), in that the periodicity of both linear and circular polarization microstructure traces closely the total power. We also investigate the spectral properties of micropulses within a sub-pulse. It is shown that the microstructure not only has a wide bandwidth, but that adjacent broad-band microstructures can have very different spectra.

1.2 Introduction

Within only a few years of the discovery of pulsar B1919+21 in 1967 it had become clear that there was great variation between individual pulses, and even structure within pulses

(Craft et al., 1968; Manchester et al., 1975; Ritchings & Lyne, 1975). Each pulsar's folded and integrated profile is highly reproducible and specific to that pulsar, however the pulses of which they are comprised are diverse in a multitude of ways (Lyne & Graham-Smith, 1998). Variation of polarization fraction and mode, intensity fluctuations of sub-pulses, and variable arrival times are examples of the pulse-to-pulse dynamics. Nulling and pulse drifting are also common, and still these ostensibly stochastic phenomena result in recognizable folded profiles. An example of this is shown in Fig. 1.1, in data taken at ARO.

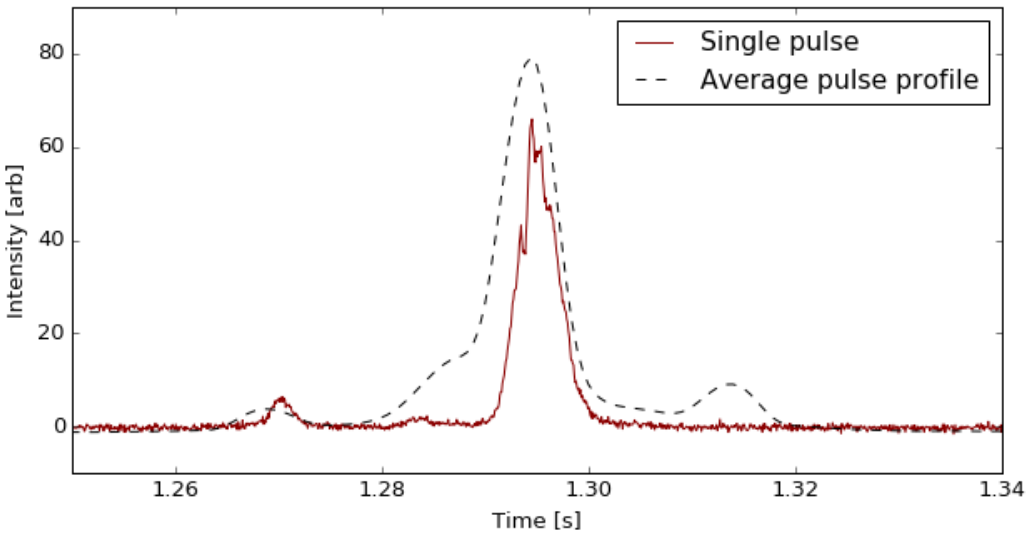

Figure 1.1: The average profile of pulsar B0329+54 (dashed, black line) plotted over a single pulse (solid, maroon line). Though there is significant variation from pulse to pulse in each of the sub-components (of which there are as many as 9 (Gangadhara & Gupta, 2001)), the average profile is well known and repeatable. It can be thought of as a probability distribution from which the power in each phase bin for a single pulse is drawn.

Understanding the physical mechanism by which pulsars emit in the radio has proven one of the hardest problems in modern astrophysics (Ginzburg & Zhelezniakov, 1975; Melrose, 2000). Most of what is known has come from folded pulse profiles, but given the substantial phenomenology on timescales of individual pulses, there is good reason

to study them.

On the shortest timescales, microstructure appears in a number of pulsars (Cordes, 1975; Lange et al., 1998). This usually involves intensity variation on sub-millisecond timescales. They can exhibit periodic oscillatory fluctuations as well as broad-band features. Although the micropulses have been seen in a number of slow pulsars at a range of frequencies, there is no agreed upon explanation for their origin (Lange et al., 1998). van Horn (1980) argued the phenomenon was not magnetospheric but rather a result of neutron star vibrations, hence the periodic nature of the substructure. Another explanation has been to evoke propagation effects in the pulsar magnetosphere. Most commonly, though, models for these micro- and millisecond intensity fluctuations have assumed it is fundamentally related to the emission mechanism rather than a separate process occurring elsewhere in the magnetosphere (Lange et al., 1998).

Before linking microstructure to broader emission mechanisms, it is useful to remind ourselves about the potential sources of radio emission in pulsars. One prominent explanation is the vacuum curvature radiation model. Curvature radiation is similar to synchrotron except with a pitch angle that is nearly zero. In the pulsar magnetosphere, this happens when electrons or positrons travel along the very strong curved magnetic field lines, radiating at some critical frequency $\nu_c \sim \gamma^3 c/r_B$, where r_B is the radius of curvature of the field lines (Lyne & Graham-Smith, 1998). Given the expected relativistic electron-positron plasma over-density at the pulsar's polar caps and the strong magnetic fields, curvature radiation seems like a natural explanation for radio emission. One difficulty with the model is that due to the exceedingly high brightness temperatures of pulsars, it has always been known that coherent emission is needed. For the vacuum curvature scenario, this requires "charged bunches" of electrons ($\sim 10^{15}$ particles) emitting coherent curvature radiation (Gil et al., 2004). It is not obvious how these bunches would be created.

The single-particle vacuum curvature-radiation model can be informed by observa-

tions microstructure and its polarization. Since the sub-pulses that make up individual pulses can be further broken down into microstructures, those microbursts should show phenomena predicted by the incoherent sum of coherently curvature emitting charged bunches (Gil & Snakowski, 1990; Mitra et al., 2015).

Few detailed polarization studies of microstructure have been carried out. Ferguson & Seiradakis (1978) commented on the qualitative polarization properties of microstructure seen in B1133+16. Kramer et al. (2002) quantitatively analyzed polarimetry observations of Vela's microstructure. Recently, however, Mitra et al. (2015) made a convincing case for studying short-timescale fluctuations of polarized pulsar emission. They observed almost three dozen sources with $\sim$60 μs time-resolution at Arecibo with periods ranging from 0.15-3.7 seconds.

1.3 B0329+54 Individual Pulses

1.3.1 Observations

The data for our B0329+54 single-pulse analysis were taken at the Algonquin Radio Observatory (ARO). The refurbished 46 m antenna was mounted with a 400-800 MHz CHIME four-leaf clover feed, the details of which are described in Chapter **??**. We attached to it a custom back-end made from CHIME hardware and software that can write voltage data to disk with $\sim$390 kHz spectral resolution and 2.56 μs temporal resolution. We refer to this as "baseband". Though the data is channelized with a polyphase filter bank (PFB), this process is invertible and we are able to de-channelize in order to coherently dedisperse offline. Data are written in the VDIF specification, similar to the Pathfinder data format described in Chapter **??**. However in the case of ARO, since we have 2 channels instead of 256, we do not need 16 FPGA boards and 16 GPU nodes to process the data. Therefore frequencies need not be reassembled because each frame contains all 1024 contiguous frequencies. There are also slight changes to the header. We

observed the pulsar for roughly 2 hours on 1 August 2014, for more than 10^4 pulses.

1.3.2 Data post-processing

We use a VLBI pulsar analysis code-base called `scintellometry`, which was built for correlating baseband data from different telescopes with differing data formats[1]. Though the code is able to coherently dedisperse, B0329+54 is slow and has a DM of only $\sim$27 pc cm^{-3}, and we have found it is sufficient to do "by-channel" dedispersion. This means stepping through each frequency of the channelized voltage data, inverse Fourier transforming that frequency's time series, and dedispersing that up-channelized chunk. The resultant DM-smearing in the case of B0329+54 is negligible.

The two dedispersed voltage time-streams are then correlated, providing four real numbers per time and frequency. Out of these correlations the Stokes parameters can be constructed. The four numbers are an autocorrelation for each polarization, and the real and imaginary components of the cross-correlation. The output array is therefore,

$$D = \begin{pmatrix} \langle X_0 X_0^* \rangle & \langle \Re e\{X_0 X_1^*\} \rangle \\ \langle \Im m\{X_0 X_1^*\} \rangle & \langle X_1 X_1^* \rangle \end{pmatrix}. \tag{1.1}$$

By rearranging these, the Stokes parameters can be obtained as follows,

$$\begin{pmatrix} \langle X_0 X_0^* \rangle & \langle X_0 X_1^* \rangle \\ \langle X_0^* X_1 \rangle & \langle X_1 X_1^* \rangle \end{pmatrix} = \begin{pmatrix} I+Q & U+iV \\ U-iV & I-Q \end{pmatrix}. \tag{1.2}$$

These intensities are either folded or written to a dedispersed time and frequency `numpy` array with arbitrary time rebinning.

Before the polarization data can be analyzed, we must remove two effects. The first is the sinusoidal phase in frequency introduced by cable delays. This comes from that fact

[1] https://github.com/mhvk/scintellometry

that the two polarizations signals, X_0 and X_1, end up with slightly different instrumental phases due to things like disparate cable lengths. When the signals are correlated, a constant phase offset (time lag) becomes a sinusoidal oscillation in frequency. Written in terms of the Stokes parameters this transformation takes,

$$X_0 X_1^* = U + iV, \tag{1.3}$$

and makes the cross-pol correlation

$$X_0 X_1^* \rightarrow (U + iV) \times e^{2\pi i \nu \tau}, \tag{1.4}$$

where τ is the instrumental time lag between the two polarizations. This rotates Stokes V into Stokes U, thereby leaking circular into linear polarization.

Another effect is Faraday rotation, which is significant for B0329+54 in our band. Its RM is $\sim$64 rad m^{-2}, resulting in several phase wraps between 400-800 MHz. Unlike cable delays, the Faraday effect rotates the linear polarization vector, P, defined by:

$$P \equiv Q + iU. \tag{1.5}$$

Similar to dispersion, it depends on λ^2. The linear polarization is rotated as,

$$P \rightarrow P\, e^{2i\,\mathrm{RM}\,\lambda^2}. \tag{1.6}$$

We remove these two effects by doing a joint fit of the folded pulse profile at each frequency. We fit for time lag, τ, RM, Stokes Q, U, and V, as well as global phase offset, ϕ_{X_0,X_1}. Though we do not do a full polarization calibration of the ARO feed, we have verified that its leakage is not too severe. This was done by measuring pulsar B1929+10, whose polarization angle swings by $\sim$80 degrees in a known way, and comparing our results to a calibrated template in the literature. We found only small deviations from

the known template.

1.4 Results

The polarization and total intensity of B0329+54 vary on a range of scales. Though the polarization in its folded profile is less than 10% for both linear and circular, the mode and fraction from individual pulses jumps around. The pol-fraction for single pulses can surpass 70%. In the ISM, scintillation causes the pulsar's brightness to fluctuate on timescales of 5-30 minutes. Between individual pulses there is variation by factors of a few, which is presumably intrinsic to the source. Within a pulse (timescales $\lesssim 50\,\mathrm{ms}$), brightness changes exist due to the multi-component nature of B0329's pulse profile. We also see sub-millisecond fluctuations within these sub-pulses. Fig. 1.2 shows such variation on minutes, seconds, and millisecond timescales respectively, going from top to bottom.

1.4.1 Quasi-periodicity

Several pulsars are known to exhibit quasi-periodic trains of micropulses. Cordes et al. (1990) found periodic variation in pulsars 0809+74, 0950+08, 1133+16, 1944+17, and 2016+28. They found that each source's microstructure had a characteristic quasi-period, and that for some pulsars the strength of microstructure scaled inversely with frequency.

In B0950+08, the periodic microstructure looks similar to Crab "nanoshots". The flux between micropulses almost entirely disappears and the bursts themselves are incredibly narrow ($\lesssim 10\,\mu\mathrm{s}$) (Popov et al., 2002). In B0329+54 we see quasi-periodic structures in a number of our strong pulses. However unlike in B0950 or the Crab, it seems to be a component that sits on top of an underlying smooth profile. To determine the timescales of this quasi-periodicity, we compute a reduced autocorrelation function (rACF). ACFs have long been used to study microstructure (see Kardashev et al., 1978; Lange et al.,

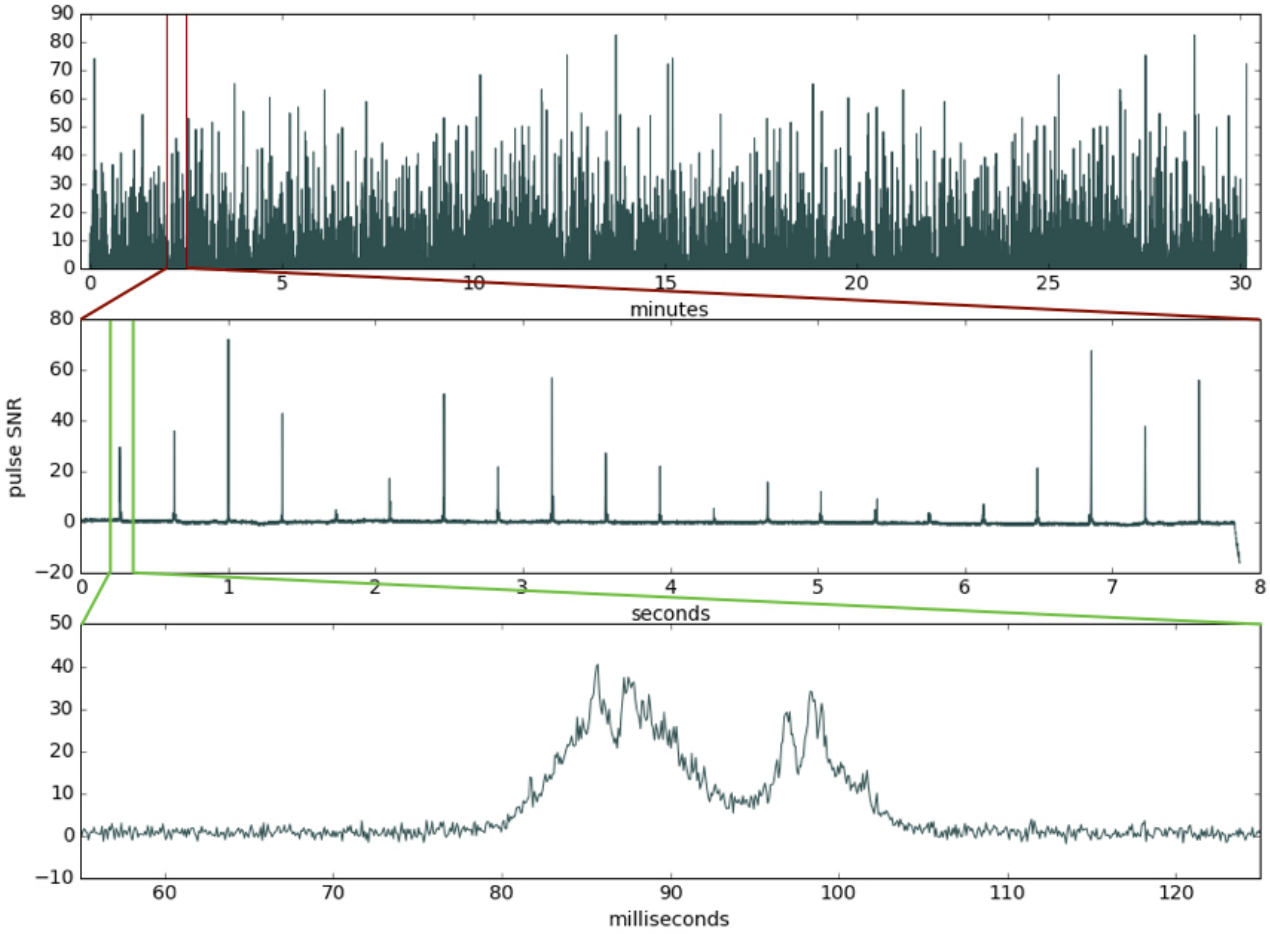

Figure 1.2: Pulsar B0329+54 intensity fluctuations on three different timescales. From top to bottom panel: roughly 2,500 pulses over a half hour; pulse-to-pulse brightness variation; and intra-pulse variation on timescales of 50 μs-10 ms.

1998). It is computed as,

$$A(\tau) \equiv \frac{\int S(t)S(t+\tau)\,\mathrm{d}t}{\int S^2(t)\,\mathrm{d}t}, \tag{1.7}$$

where $S(t)$ is any time-stream intensity, whether Stokes I, Q, U, or V. The maxima, minima, and slope changes of $A(\tau)$ can inform us about relevant timescales in the pulse (Mitra et al., 2015).

For pulsars like B0329+54 whose microstructure often sits on top of a smoother pulse profile, $A(\tau)$ does not exhibit obvious structure. To avoid this problem we fit each subpulse with a Gaussian, subtract that off, then calculate the "reduced" ACF using,

$$S'(t) \rightarrow S(t) - \mathcal{N}(\mu_{\rm fit}, \sigma^2_{\rm fit}). \tag{1.8}$$

An example of this is shown in the Fig. 1.3. The left panels shows bright single pulses with a trains of microbursts for both $S(t)$ and $S'(t)$. The right panel shows the corresponding ACFs. The black curve is the rACF, since it is the autocorrelation of a Gaussian-subtracted pulse.

There is a known correlation between microstructure timescales and the pulsar period. Kramer et al. (2002) have shown the scaling to be,

$$t_\mu \approx 6 \times 10^{-4} P, \tag{1.9}$$

where P is the pulsar's period and t_μ is the timescale of individual microbursts, often estimated by the first local minimum in the ACF. This was consistent with the original claim by Cordes & Hankins (1979). Mitra et al. (2015) used 24 L-band pulsars to revisit the relationship. Instead of using t_μ, they used the period of quasi-periodic microstructure, T_μ, and found it too increased with pulsar period as $\sim 10^{-3} P$. Here we will follow suit and focus primarily on the first local maximum. The reason we use this rather than widths of individual microbursts is because those are often unresolved in time or scattered by the ISM.

For B0329+54 we find the absence of a characteristic timescale, but consistency with the known $t_\mu-$ and $T_\mu - P$ relation. In Fig. 1.3 we show an illustrative example of the differences in microstructure timescales from pulse to pulse. The top row's pulse has $t_\mu \sim 0.28\,$ms and $T_\mu \sim 0.55\,$ms, whereas the bottom row's pulse has $t_\mu \sim 0.68\,$ms and $T_\mu \sim 1.2\,$ms. For B0329+54 we expect the first minima of rACFs to be around $400\,\mu$s

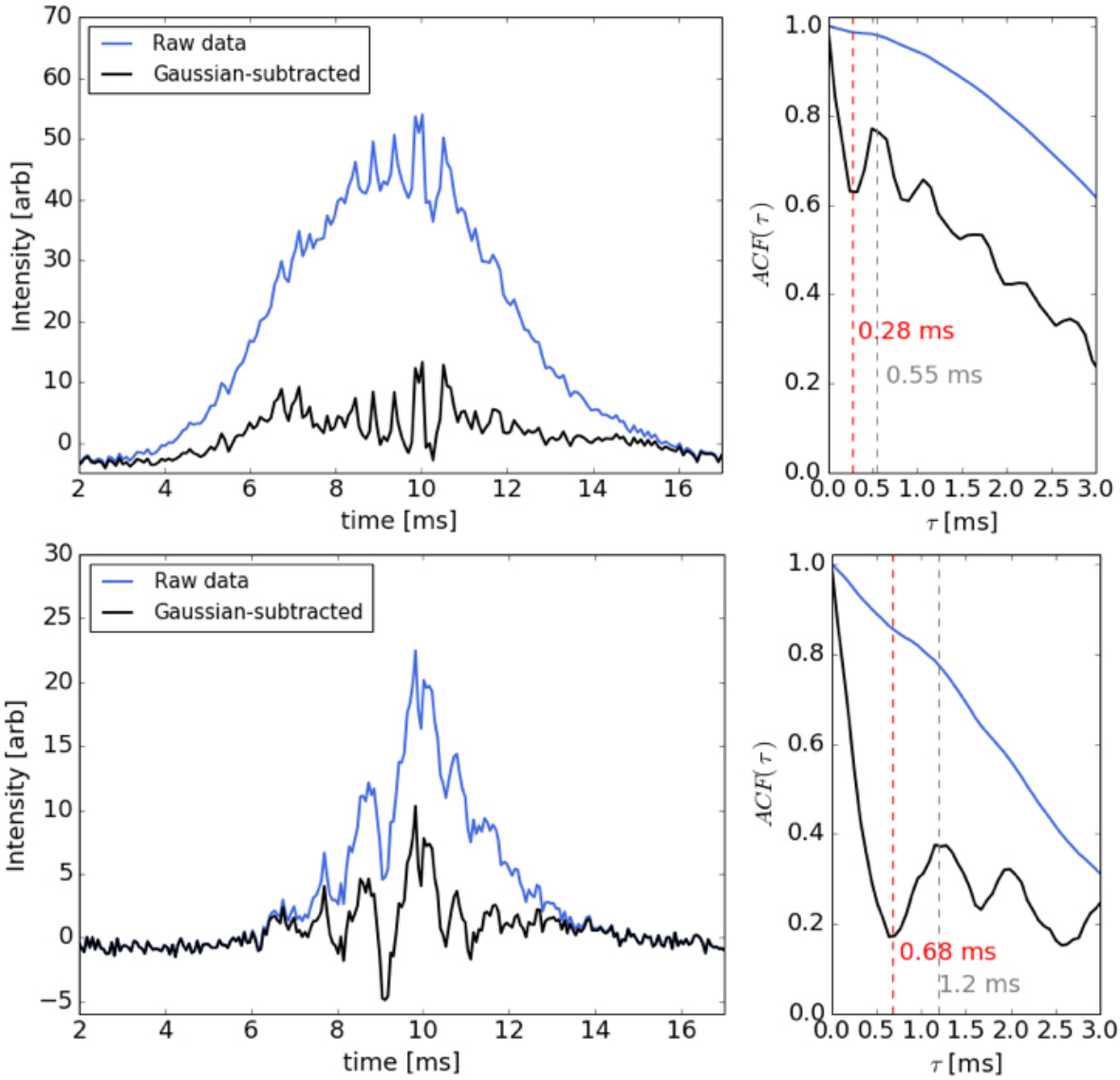

Figure 1.3: Periodicity and quasi-periodicity seen in microstructure from two individual B0329+54 pulses. The top left panel shows a pulse with a periodic train of microbursts for both the raw profile (slate blue) and the Gaussian-subtracted profile (black). The bottom left panel shows broader and more moduluated quasi-periodic microstructure. The right panels show the corresponding ACF (slate blue) and rACF (black). There are two striking features about these plots. The first is that unlike other pulsars that exhibit microstructure, B0329+54 does not seem to have a characteristic period or width to its structure. This is seen by comparing the first minima and maxima of the correlation functions and noticing they are at different timescales for the two pulses. The second is that the correlation function contains very little information if a smooth component is not first subtracted, i.e., if the rACF is not computed.

and the first maxima to be at 700 μs. In general, we find a range of $t_\mu \sim 100 - 1000\,\mu$s and $T_\mu \sim 500 - 2000\,\mu$s, which are consistent with the trend seen in other pulsars.

There are two basic ways to get sub-millisecond variations in pulsars: angular beaming in the direction transverse to the observer, and actual temporal modulation in the magnetosphere. To interpret our measured timescales, we can start in the framework of a beaming model, in which the width of a micropulse is given by a radiating point source with some Lorentz factor, γ. If we take t_μ as an upper limit for the width of a microburst, the pulse's width in radians is at least,

$$\phi = 2\pi\, t_\mu / P. \tag{1.10}$$

The Lorentz factor will be given by,

$$\gamma = \frac{1}{\phi \sin\delta}, \tag{1.11}$$

where δ is the angle between the pulsar's rotation axis and the line of site (Lange et al., 1998). Our results give a lower-limit on γ of ∼200-1000. This is difficult to reconcile with several theoretical studies, which suggest the particles producing microstructure should have $\gamma < 100$ (Asseo et al., 1992; Lange et al., 1998).

Polarization

1.4.2 Microburst spectral variation

In some of the brightest pulses we find frequency variation between individual microbursts. Given the timescales invovled (200-1500 μs), such variation is not expected to be due to propagation effects like scintillation. The top right panel of Fig. 1.5 shows the same pulse at 450 MHz (red) and 640 MHz (black). We isolate three brightest individual micropulses shaded by light blue, blight red, and grey. One can see the light blue pulse is quite bright at 640 MHz, but less so at 450 MHz. The light grey pulse almost completely

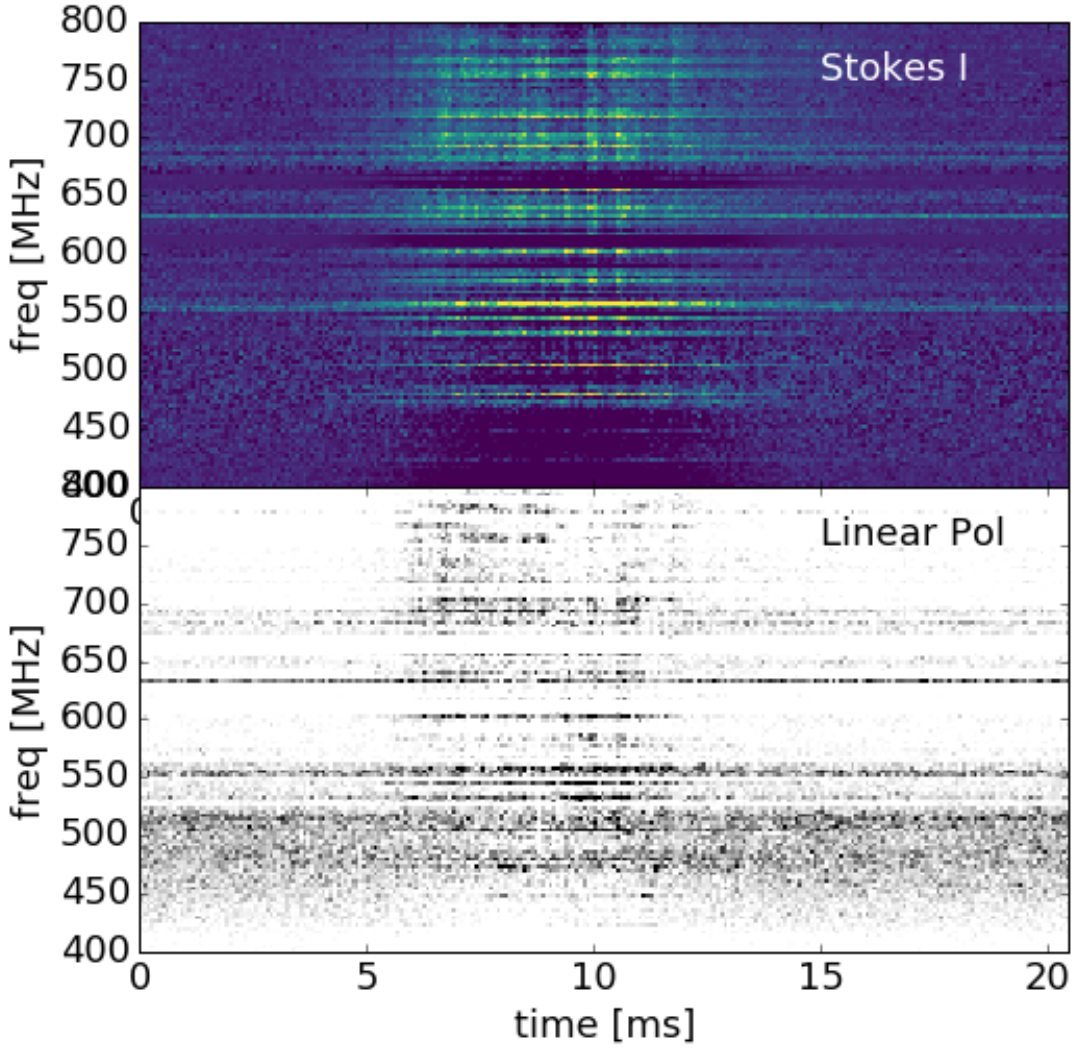

Figure 1.4:

disappears by 640 MHz, even though it is prominent at lower frequencies. The light red microburst is somewhere between the other two.

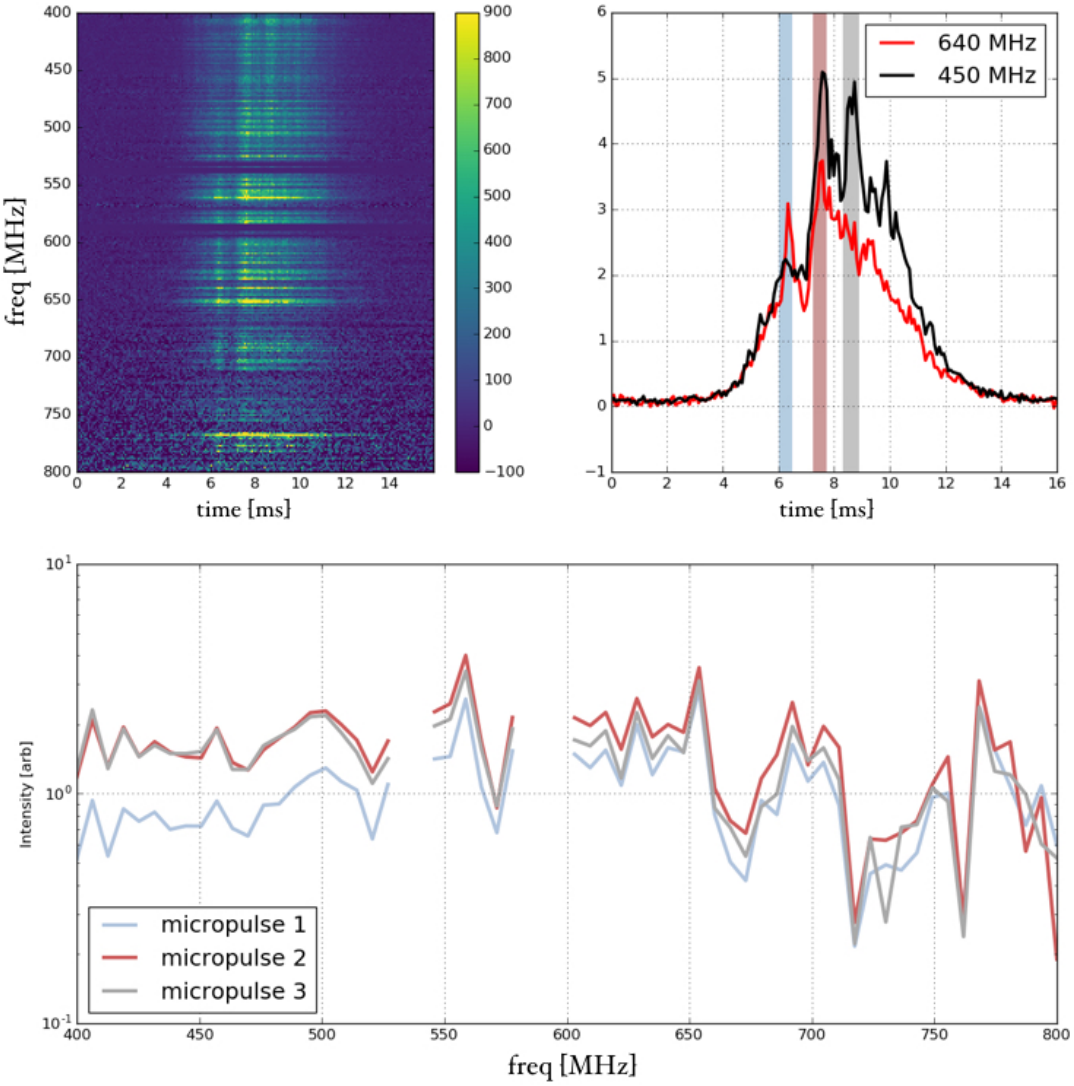

Figure 1.5: An example of broad-band microstructure in a particularly bright pulse. This pulse's three most prominent microbursts have very different frequency behaviour. *top left:* Frequency time colour map showing this pulse over the full band, for roughly 15 ms. The broad-band nature of the microstructure is also apparent as vertical pipe-like structures. *top right:* Pulse profile for two different frequencies: centered on 640 MHz and 450 MHz, averaged over ∼40 MHz. The three vertical shaded regions, blue, red, and grey, correspond to the three brightest micropulses, "micropulse 1", "micropulse 2", "micropulse 3", respectively. One can also see their differences in their spectral behaviour. The first spike is brighter at 450 MHz than at 640 MHz, but the opposite is true of the second and third spikes. *bottom panel:* The relative spectra of three micropulses, with colours corresponding to the shaded region in the top right panel. In order to compare the frequency structure more easily, the off-pulse (any RFI or Galaxy in the beam) was subtracted, and the averaged pulse profile of B0329+54 was divided out.

1.5 Conclusion

We have presented analysis of the largest collection of microsecond-resolution single-pulse data of B0329+54. Broadband microstructure was found to be a standard property of this pulsar, although it is rarely highly modulated. The sub-pulses we analyzed often exhibited quasi-periodic trains of micropulses. We quantified such periodicity with a reduced autocorrelation function, which pulls out time-like correlations by first removing the stronger, smooth component of the sub-pulse. The quasi-periodic microstructure of B0329+54 were found to have no characteristic timescale, which is different from other pulsars that have been studied. However, we did show that the range of periods are consistent with the known $T_\mu \approx 10^{-3}\,P$ relation. The micropulse widths are also roughly consistent with the known $t_\mu - P$ scaling.

The microburst widths allow us to estimate the Lorentz factor of the radiating particles, assuming the widths are due to relativistic beaming. We find $\gamma \sim 200 - 1000$, which are inconsistent with the expected velocities. This inconsistency was also found by Lange et al. (1998), who use it to reject the beaming model.

Bibliography

Asseo, E., Pelletier, G., & Sol, H. 1992, in IAU Colloq. 128: Magnetospheric Structure and Emission Mechanics of Radio Pulsars, ed. T. H. Hankins, J. M. Rankin, & J. A. Gil, 322

Cordes, J. M. 1975, PhD thesis, California Univ., San Diego.

Cordes, J. M., & Hankins, T. H. 1979, ApJ, 233, 981

Cordes, J. M., Weisberg, J. M., & Hankins, T. H. 1990, AJ, 100, 1882

Craft, H. D., Comella, J. M., & Drake, F. D. 1968, Nature, 218, 1122

Ferguson, D. C., & Seiradakis, J. H. 1978, A&A, 64, 27

Gangadhara, R. T., & Gupta, Y. 2001, ApJ, 555, 31

Gil, J., Lyubarsky, Y., & Melikidze, G. I. 2004, ApJ, 600, 872

Gil, J. A., & Snakowski, J. K. 1990, A&A, 234, 269

Ginzburg, V. L., & Zhelezniakov, V. V. 1975, ARA&A, 13, 511

Kardashev, N. S., Kuzmin, A. D., Nikolaev, N. I., et al. 1978, AZh, 55, 583

Kramer, M., Johnston, S., & van Straten, W. 2002, MNRAS, 334, 523

Lange, C., Kramer, M., Wielebinski, R., & Jessner, A. 1998, A&A, 332, 111

Lyne, A. G., & Graham-Smith, F. 1998, Pulsar astronomy

Manchester, R. N., Taylor, J. H., & Huguenin, G. R. 1975, ApJ, 196, 83

Melrose, D. B. 2000, in Astronomical Society of the Pacific Conference Series, Vol. 202, IAU Colloq. 177: Pulsar Astronomy - 2000 and Beyond, ed. M. Kramer, N. Wex, & R. Wielebinski, 721

Mitra, D., Arjunwadkar, M., & Rankin, J. M. 2015, ApJ, 806, 236

Popov, M. V., Bartel, N., Cannon, W. H., et al. 2002, Astronomy Reports, 46, 206

Ritchings, R. T., & Lyne, A. G. 1975, Nature, 257, 293

van Horn, H. M. 1980, ApJ, 236, 899